

# Tailoring the Surface of NiTi Alloy Using PIRAC Nitriding Followed by Anodization and Phosphonate Monolayer Deposition

Gilad Zorn,<sup>†</sup> Racheli Adadi,<sup>‡</sup> Reuven Brenner,<sup>§</sup> Vladimir A. Yakovlev,<sup>||</sup> Irena Gotman,<sup>†</sup> Elazar Y. Gutmanas,<sup>†</sup> and Chaim N. Sukenik<sup>\*‡</sup>

Faculty of Materials Engineering, Technion, Haifa, Israel 32000, The Department of Chemistry and The Nano-Medicine Center of the Bar Ilan Institute for Nanotechnology and Advanced Materials, Bar-Ilan University, Ramat-Gan, Israel 52900, Solid State Institute, Technion, Haifa, Israel 32000, and Institute of Spectroscopy, RAS, 142190 Troitsk, Moscow Region, Russia

Received December 31, 2007. Revised Manuscript Received June 11, 2008

Nickel titanium (NiTi, nitinol) shape memory alloy was nitrided using a powder immersion reaction assisted coating (PIRAC) method to modify its surface properties. PIRAC nitriding is based on annealing the samples in an atmosphere of highly reactive nitrogen supplied by decomposition of unstable nitride powders or, alternatively, by selective diffusion of atmospheric nitrogen to the sample surface. Since it is not line of sight limited, PIRAC nitriding of nitinol alloys allows uniform treatment of complex shapes (e.g., surgical implants). It results in the formation of a Ni-free TiN film and considerably improves the corrosion behavior of the underlying NiTi alloy. The usefulness of PIRAC nitrided nitinol could be significantly enhanced by attaching to its surface a phosphonate anchored self-assembled monolayer (SAM). Phosphonate-anchored SAMs on PIRAC nitrided nitinol and on thin films of TiN sputtered onto a silicon wafer have been characterized by FTIR, contact angle measurements, and XPS analysis. The SAM was only weakly attached to the nitride surface. However, when anodization was used to add an oxide layer on top of the TiN, a robust, uniform phosphonate-anchored SAM could be formed. Thus, anodization of the nitride surface allows it to continue functioning as a corrosion barrier while still being able to take advantage of the range of surface chemistries offered by SAM films. The composition and morphology of the nitrided TiNi surface, before and after anodization, are reported, along with an analysis of phosphonate-anchored SAM formation on these surfaces.

## Introduction

NiTi (Nitinol) is an equiatomic intermetallic compound of nickel and titanium whose unique mechanical properties (thermal shape memory, superelasticity, and low elastic modulus) contribute to its increasing use as a biomaterial.<sup>1</sup> Despite several successful clinical applications, the biocompatibility of NiTi still remains controversial. Released nickel ions may promote toxic, allergic, and potentially carcinogenic effects, and specific concerns have been raised regarding the corrosion behavior of nickel-containing alloys in general and NiTi in particular.<sup>1–5</sup>

Recently it has been shown that Ni release from NiTi can be significantly reduced by PIRAC nitriding.<sup>6</sup> The process produces a thin TiN layer on the NiTi surface that improves the alloy corrosion behavior and acts as a diffusion barrier for Ni ions. Such TiN-coated NiTi may become sufficiently

bioinert to allow direct apposition of the bone tissue when placed in the bony environment. A robust implant–tissue interface, however, will not be developed unless the material has the ability to guide initial cellular reactions at the implant site. This may be achieved through implant biofunctionalization, incorporation of molecular signaling functionalities having a proven influence on bone cell behavior.

One promising biofunctionalization strategy is the grafting of biomaterial surfaces with peptides simulating the cell-binding ability of the extra-cellular matrix (ECM). Self-assembled monolayers (SAMs) that provide chemically and structurally well-defined organic coatings can be useful for such peptide attachment.<sup>7–9</sup> Self-assembly of an organic monolayer on a metal or alloy surface depends in large part on the composition and reactivity of the surface. For oxide-coated metals including Ti alloys, successful SAM attachment has been reported using both siloxane and phosphonate “head groups”.<sup>10,11</sup> Recently, successful installation of phos-

<sup>†</sup> Faculty of Materials Engineering, Technion.

<sup>‡</sup> Bar-Ilan University.

<sup>§</sup> Solid State Institute, Technion.

<sup>||</sup> RAS.

- (1) Shabalovskaya, S. A. *Int. Mater. Rev.* **2001**, *46* (5), 233–250.
- (2) Wever, D. J.; Veldhuizen, A. G.; Sanders, M. M.; Schakenraad, J. M.; van Horn, J. R. *Biomaterials* **1997**, *18*, 1115–1120.
- (3) Ryhanen, J.; Niemi, E.; Serlo, W.; Niemela, E.; Sandvik, P.; Pernu, H.; Salo, T. J. *Biomed. Mater. Res.* **1997**, *35*, 451–457.
- (4) Maitz, M. F.; Shevchenko, N. J. *Biomed. Mater. Res., Part A* **2006**, *76A*, 356–365.
- (5) Tan, L.; Dodd, R. A.; Crone, W. C. *Biomaterials* **2003**, *24*, 3931–3939.
- (6) Starosvetsky, D.; Gotman, I. *Biomaterials* **2001**, *22*, 1853–1859.

- (7) Zorn, G.; Gotman, I.; Gutmanas, E. Y.; Adadi, R.; Sukenik, C. N. *J. Mater. Sci.: Mater. Med.* **2007**, *18*, 1309–1315.
- (8) Schwartz, J.; Avaltroni, M. J.; Danahy, M. P.; Silverman, B. M.; Hanson, E. L.; Schwarzbauer, J. E.; Midwood, K. S.; Gawalt, E. S. *Mater. Sci. Eng.* **2003**, *C23*, 395–400.
- (9) Rezanian, A.; Johnson, R.; Lefkowitz, A. R.; Healy, K. E. *Langmuir* **1999**, *15*, 6931–6939.
- (10) Zorn, G.; Gotman, I.; Gutmanas, E. Y.; Adadi, R.; Salitra, G.; Sukenik, C. N. *Chem. Mater.* **2005**, *17*, 4218–4226.
- (11) Gawalt, E. S.; Avaltroni, M. J.; Koch, N.; Schwartz, J. *Langmuir* **2001**, *17*, 5736–5738.

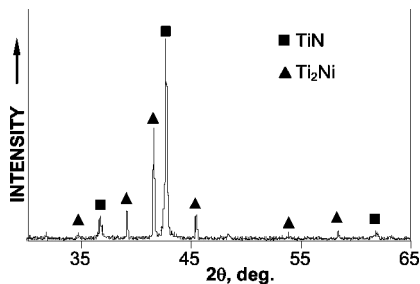


**Figure 1.** XRD analysis of PIRAC nitrated NiTi: diffraction peaks of TiN and Ti<sub>2</sub>Ni (as per JCPDS card nos. 38-1420 and 18-898) are marked. Note: the peak at ~43° is likely enhanced by diffraction from the NiTi substrate (JCPDS card no. 18-899).

phosphate anchored SAMs on NiTi surfaces has been reported.<sup>12,13</sup> The latter approach seems more attractive for developing stable interfaces to bind biomolecules since, unlike siloxanes, phosphonate interfaces are stable to hydrolysis at physiological pH and their fabrication is not limited by low native oxide surface OH group content.<sup>8,14</sup> Moreover, phosphonic acids are easier to handle and have better long-term stability than the hydrolyzable silanes needed to form siloxane anchored SAMs.

Given the benefits of nitriding in terms of the biocompatibility of NiTi and considering the need to use the nitride layer to provide corrosion protection, the attachment of alkylphosphonate SAMs to the nitride surface is a potentially useful way to benefit from both the nitride and the SAM coating. However, SAM anchoring on the nitrated surface has never been reported. The main thrust of the present work, therefore, was to evaluate the ability of PIRAC-nitrated NiTi to support the attachment and self-assembly of hexadecylphosphonic acid (HDPa) using the procedure reported for HDPa SAM deposition on oxidized Ti45Nb alloy.<sup>10</sup> Once the difficulty of forming a well-packed phosphonate SAM on the nitrated surface was established a procedure to create an oxide layer on the nitrated NiTi surface was developed. In this report, we compare the phosphonate SAMs obtained on the nitride surface to that obtained when the nitride is first anodized/oxidized. The SAMs were extensively characterized, and the HDPa attachment capability of the

two surface chemistries was compared. Ultimately, the ability to achieve effective SAM coating on the anodized nitride surface provides an excellent opportunity to enjoy the advantages of both of these surface modification tools in the search for ways to improve the biocompatibility and utility of NiTi.

## Materials and Methods

1. NiTi Alloy (purchased from Performance Materials and Alloys, U.S.A., 1 × 1 cm<sup>2</sup>; sample thickness 3 mm) samples were first subject to grinding with with 60, 120, 240, and 600 grit silicon carbide paper, followed by diamond polishing (6, 3, 1, and 1/4 μm particle sizes). The samples were sonicated in acetone and then in ethanol (15 min each) and dried in a stream of dry nitrogen.

The samples were then PIRAC nitrated by annealing in stainless steel containers at 1000 °C for 1 or 12 h. To prevent direct contact with the container walls, the samples were immersed in TiN powder. The container steel contained 26 wt % Cr that reacted on heating with the atmospheric oxygen forming a very stable Cr<sub>2</sub>O<sub>3</sub> oxide. This reaction prevented oxygen from penetrating into the container. Unlike oxygen, atmospheric nitrogen easily diffused through the container walls due to its rather low affinity for Cr and reacted with NiTi forming a layer of Ni-free titanium nitride on the sample surface.<sup>15</sup>

Samples of NiTi that had been PIRAC nitrated for 12 h (having a correspondingly thicker nitride coating) were anodically oxidized in a 1 M H<sub>2</sub>SO<sub>4</sub> electrolyte at room temperature. The current density was kept at 60 mA/cm<sup>2</sup> during the initial part of anodization while the potential was allowed to increase from 5 V to a preset value of 50 V. When the preset voltage was reached, (after about 1 min) the anodization was stopped.

The nitrated and anodized samples were sonicated successively in acetone, DI water, and ethanol (15 min each) and then dried in a stream of dry air.

As a more readily analyzed model for the TiN formed on the nitinol surface, a thin (20 nm) titanium nitride film was sputtered onto a single crystal {100} silicon wafer using a Veeco Ion Beam Deposition System (Semiconductor Devices LTD, Israel).

2. For monolayer deposition, HDPa (17 mg) was dissolved in THF (40 mL) and heated (with stirring) to 70 °C under nitrogen. Samples were immersed into this solution and kept at 70 °C for 2 h after which the temperature was raised to 100 °C causing THF

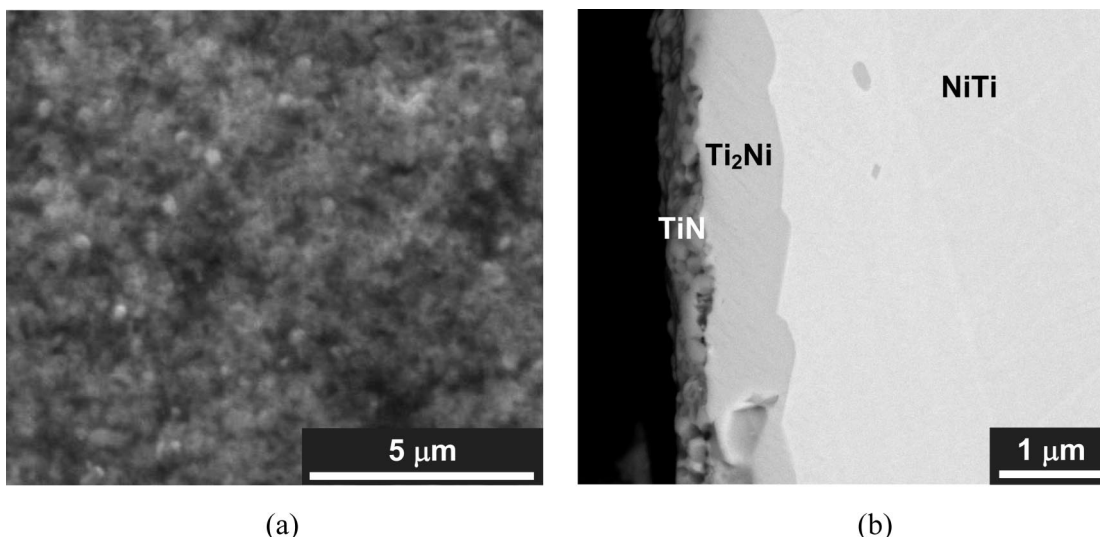


**Figure 2.** SEM images of PIRAC nitrated NiTi at 1000 °C, 1 h: (a) top view; (b) cross section.

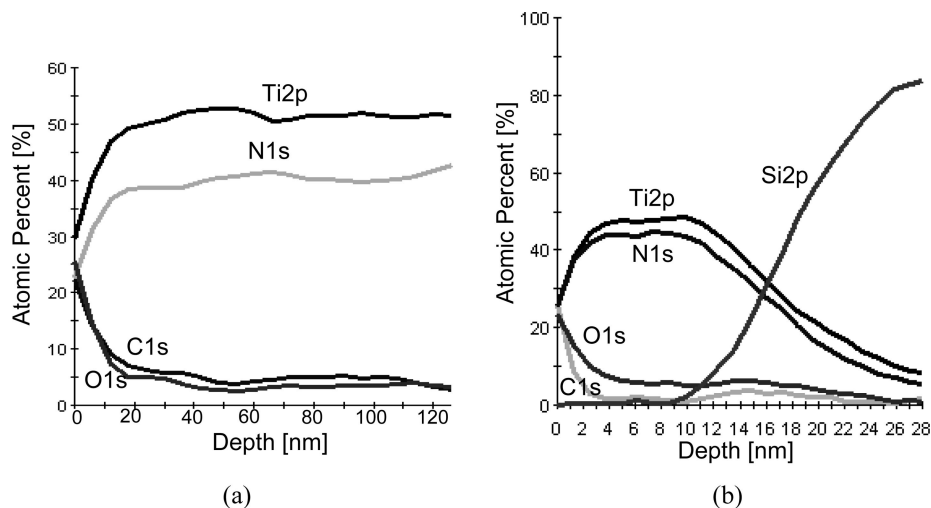


Figure 3. XPS depth profiles of (a) PIRAC nitrided NiTi and (b) TiN-sputtered on a silicon wafer.

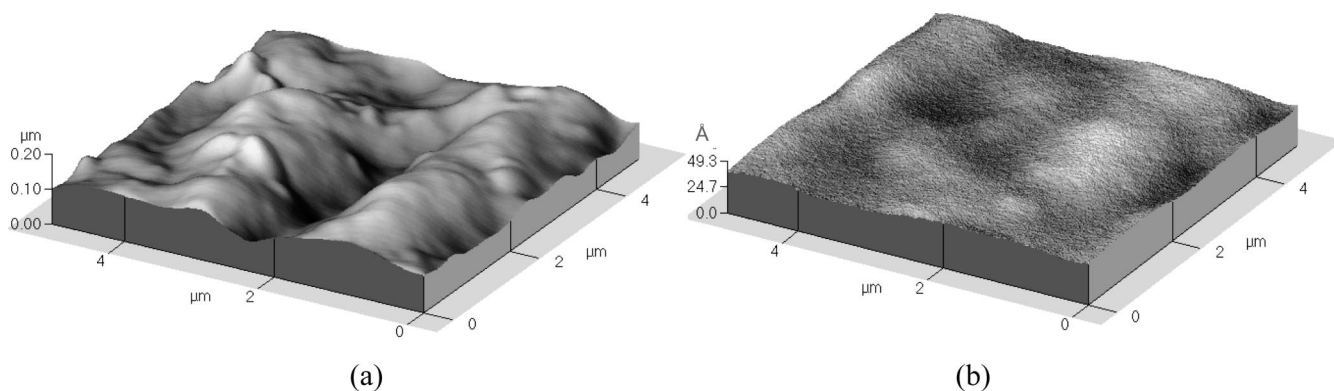


Figure 4. AFM 3D images of PIRAC nitrided NiTi at 1000 °C, 1 h (a) and TiN-sputtered on a silicon wafer (b).

Table 1. XPS Surface Composition of PIRAC Nitrided NiTi, of Sputtered TiN on a Si Wafer, and of Anodized PIRAC-Nitrided NiTi

element	atomic concentration (%)		
	PIRAC nitrided NiTi	sputtered TiN on Si	anodized PIRAC nitrided NiTi
C	36.8	28.7	28.0
O	22.0	29.3	53.2
Ti	20.4	21.5	17.5
N	20.8	20.6	1.3

to boil out (~2 h). The samples were left open to air at 100 °C for an additional 16 h. They were rinsed in fresh, dry THF and then dried with filtered N<sub>2</sub> and characterized.

3. Scanning electron microscopy (SEM) images were taken in a Quanta SEM (Oxford Instruments, U.K.).

4. Atomic force microscope (AFM) measurements were performed with an Autoprobe CP AFM (Park Scientific Instruments, U.S.A.) operated in the contact mode. AFM scans were done with CS11/50 Ultrasharp Si tips, coated with W<sub>2</sub>C. Their nominal radius of curvature was 50 nm. Scan rate was 1 line/s. The AFM images contained 256 × 256 pixels. The average surface roughness (*R<sub>a</sub>*) was calculated using ProScan Image Processing (PSI) software.

5. X-ray photoelectron spectroscopy (XPS) analyses were performed in a Sigma probe X-ray photoelectron spectrometer (Thermo VG Scientific, U.K.) using a monochromatized Al K $\alpha$  (1486.68 eV) excitation. Spectra were taken at a 37 ± 30° takeoff angle with respect to the surface. Samples were analyzed with a pass energy of 100.0 and 20.0 eV for survey and high energy

resolution elemental scans, respectively. The energy scale was calibrated by referencing the main hydrocarbon peak of C 1s at a binding energy of 285.0 eV. Gaussian/Lorentzian curve deconvolution of high energy resolution lines was done by using the XPSPEAK 4.1 software, after Shirley background subtraction. Depth profiling was done using 4 keV Ar<sup>+</sup> ions, and the depth scale was calibrated using a 100 nm Ta<sub>2</sub>O<sub>5</sub> standard.

6. X-Ray diffraction (XRD) analysis was performed using a Philips-PW-1820 Bragg–Brentano geometry diffractometer equipped with a Cu tube operated at the accelerating voltage of 40 kV and filament electric current of 40 mA.

7. For contact-angle measurements, advancing and receding water contact angle values (average of at least five measurements taken at different points on the surface) were measured using a Ramehart model 100 contact angle goniometer.

8. Fourier transform infrared (FTIR) spectroscopy measurements were done in the Institute of Spectroscopy of the Russian Academy of Sciences using a Bruker IFS66v/s infrared Fourier transform spectrometer with reflection unit at 60° angle of incidence in p-polarized light. A pyro-electric TGS detector with KBr window was used. Number of scans was 500 for background (mirror) and 256 for the samples; spectral resolution was 2 cm<sup>-1</sup>.

## Results and Discussion

**Characterization of PIRAC Nitrided NiTi.** PIRAC nitriding yielded a characteristic golden-colored titanium nitride coating on the NiTi surface. According to the XRD

results (Figure 1) the nitrated NiTi surface contains TiN and a Ti-rich intermetallic,  $Ti_2Ni$ . While the TiN is formed at the top of the nitride layer, the  $Ti_2Ni$  is between the TiN and the bulk NiTi (Figure 2). After 1 h of PIRAC treatment at 1000 °C, the thicknesses of the TiN and  $Ti_2Ni$  layers are 0.4 and 0.8  $\mu m$ , respectively. According to the XPS depth profile (Figure 3a) no Ni is present in the surface layer to a depth of at least 100 nm. This feature of the PIRAC TiN coating is very attractive for biomedical applications of NiTi since it should prevent Ni ion release into the body fluids. The presence of oxygen close to the surface is also noteworthy suggesting that the topmost layer of the PIRAC coating is some kind of oxide–nitride mixture rather than a pure TiN.

The average roughness,  $R_a$ , of PIRAC nitrated NiTi as determined by AFM (Figure 4a) was 44 nm. Such a high roughness of the real-world alloy limits our ability to analyze the monolayer to be deposited. To overcome this problem, a smooth model sample of TiN on a polished silicon wafer was used. This allows for an accurate characterization of the nitride layer and its organic coating while preserving the relevant surface characteristics.

**Surface Analysis of TiN-Coated NiTi and TiN Layer Sputtered onto Si.** It is important to verify that the composition of the model TiN surface is similar to that of the real-world nitrated NiTi. Ion beam deposition of TiN on the surface of a single crystal silicon wafer produced very smooth and uniform surface layers (Figure 4b) with the average roughness of 4.6 Å (a factor of 100 smoother than the real-world material). The effect of surface roughness on the wetting behavior of TiN was observed, with lower contact angle values measured for PIRAC nitrated NiTi ( $adv/rec = 48/45 \pm 4^\circ$ ) versus sputtered TiN on silicon ( $55/46 \pm 2^\circ$ ). This is in agreement with the Wenzel approach<sup>16</sup> stating that contact angles of  $<90^\circ$  measured on smooth surfaces will decrease with increasing surface roughness.

XPS was used to analyze and compare the surface compositions of PIRAC nitrated NiTi substrates and of the TiN layer sputtered onto the silicon wafers. As can be seen in Figure 3 and Table 1, the two surfaces contained comparable amounts of Ti, nitrogen, oxygen, and carbon contamination. Another important observation is that the corresponding spectra of Ti 2p and N 1s from the two types of samples had similar line shapes and could be deconvoluted into the same peaks (Figure 5 and Table 2). The deconvolution procedure indicated that, in addition to the nitride phase, both PIRAC-grown and sputtered TiN contained Ti dioxide ( $TiO_2$ ) and Ti oxynitride ( $TiN_xO_y$ ).

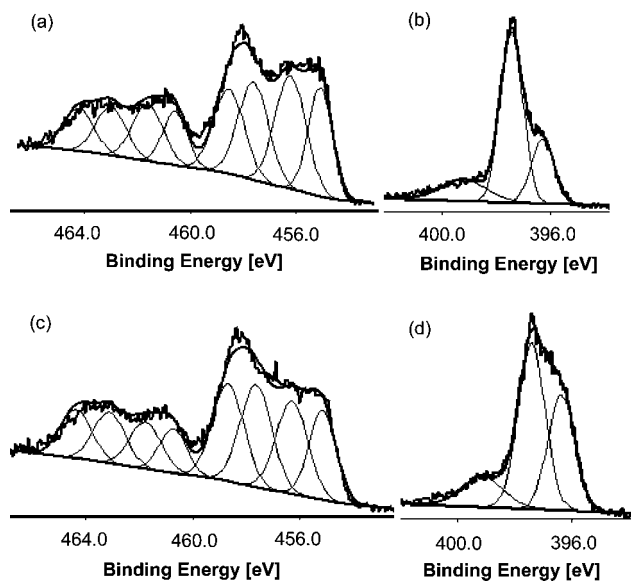


**Figure 5.** High resolution XPS spectra of Ti 2p and N 1s measured from (a, b) PIRAC nitrated NiTi and (c, d) TiN sputtered on a silicon wafer.

**Table 2.** Ti 2p<sub>3/2</sub>, N 1s, and O 1s XPS Binding Energies, Full Widths at Half Maximum (FWHM), and Ratios of Deconvoluted Components for NiTi after PIRAC Nitriding vs Sputtered TiN on a Silicon Wafer

	binding energy FWHM		assignment <sup>17–19</sup>	PIRAC nitrated sputtered	
	[eV]	[eV]		NiTi	TiN
Ti 2p <sub>3/2</sub>	455.1 ± 0.1	1.2	Ti nitride	0.23	0.21
	456.2 ± 0.1	1.4	Ti oxynitride I	0.29	0.25
	457.6 ± 0.1	1.4	Ti oxynitride II	0.26	0.28
	458.6 ± 0.1	1.3	TiO <sub>2</sub>	0.22	0.26
N 1s	396.3 ± 0.1	1.2	Ti oxynitride	0.23	0.30
	397.4 ± 0.1	1.1	Ti nitride	0.59	0.51
	399.2 ± 0.1	1.7	contamination	0.18	0.19
O 1s	530.1 ± 0.1	1.4	TiO <sub>2</sub>	0.46	0.56
	531.6 ± 0.1	1.6	Ti oxynitride, OH	0.35	0.33
	533.3 ± 0.1	1.7	contamination	0.19	0.11

The Ti 2p spectra of the two types of samples are fitted using four peaks (Figure 5a,c). The peaks at 455.1 and 458.6 eV are assigned, correspondingly, to TiN and TiO<sub>2</sub>, while the other two peaks (at 456.2 and 457.6 eV) are assigned to two Ti oxynitrides ( $TiN_xO_y$ ). The presence of two distinct oxynitride peaks suggests that the surface layer contains  $TiN_xO_y$  of at least two different stoichiometries. The shapes of XPS lines in Figure 5 along with the higher amount of oxygen in the sputtered TiN layer (Table 1) indicate that the latter contains somewhat higher amounts of the oxide and oxynitride phases compared to the TiN coating PIRAC-grown on NiTi alloy.

On the whole, the results of XPS analysis of our TiN substrates are comparable with the literature data on TiN coatings<sup>20,21</sup> and are consistent with a topmost surface that is a mixture of Ti oxynitride and TiO<sub>2</sub> and a TiN layer underneath. The surface composition of the smooth TiN-sputtered silicon wafer is almost identical to that of PIRAC nitrated NiTi alloy, making it a good model for the real material and a useful tool for studying organic film attachment.

**HDBA Attachment to the TiN Surface.** Water contact angles measured on HDBA-treated PIRAC TiN-coated NiTi

(12) Pizem, H. Ph.D. Thesis, Bar-Ilan University, 2003.  
 (13) Quinones, R.; Gawalt, E. S. *Langmuir* **2007**, *23*, 10123–10130.  
 (14) Silverman, B. M.; Wieghaus, K. A.; Schwartz, J. *Langmuir* **2005**, *21*, 225–228.  
 (15) Starosvetsky, D.; Gotman, I. *Surf. Coat. Technol.* **2001**, *148*, 268–276.  
 (16) Wenzel, R. N. *Ind. Eng. Chem.* **1936**, *28*, 988–994.  
 (17) Saha, N. C.; Tompkins, H. G. *J. Appl. Phys.* **1992**, *72*, 3072–3079.  
 (18) Milošev, I.; Strehblow, H. H.; Navinšek, B.; Metikoš-Huković, M. *Surf. Interface Anal.* **1995**, *23*, 529–539.  
 (19) Bertóti, I.; Mohai, M.; Sullivan, J. L.; Saied, S. O. *Appl. Surf. Sci.* **1995**, *84*, 357–371.

(20) Zerkout, S.; Achour, S.; Mosser, A.; Tabet, N. *Thin Solid Films* **2003**, *441*, 135–139.  
 (21) Bertóti, I. *Surf. Coat. Technol.* **2002**, *151–152*, 194–203.

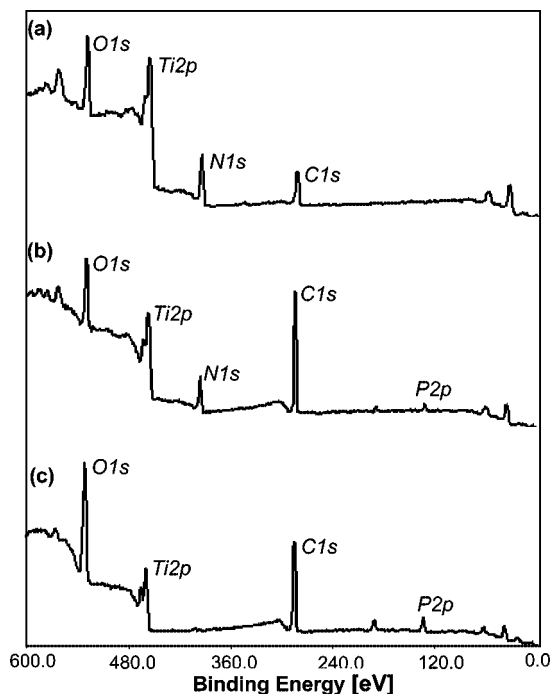


**Figure 6.** XPS survey spectra of (a) PIRAC nitrated NiTi, (b) HDPA treated PIRAC nitrated NiTi, and (c) HDPA treated anodized PIRAC nitrated NiTi.

were  $111 \pm 4^\circ$  and  $99 \pm 4^\circ$ , for the advancing and receding angles, respectively. There is precedent for alkyl monolayers on nonsingle crystal substrates with advancing contact angles of  $\geq 108^\circ$ .<sup>22,23</sup> At the same time, noticeably lower contact angle values ( $103/95 \pm 2^\circ$  adv/rec) were obtained for HDPA-treated TiN on Si wafers, suggesting that the wetting behavior of our real-world NiTi alloy was affected by its high roughness (as per Wenzel<sup>16</sup>) and that the HDPA monolayer formed on a TiN-coated surface is in fact not a well-ordered SAM.

Consistent with this are the XPS spectra of a nitrated NiTi before (Figure 6a) and after (Figure 6b) deposition of HDPA on its surface. The phosphorus signal observed in Figure 6b is consistent with the presence of surface adsorbed/attached HDPA molecules. The more prominent carbon signal and the weaker Ti and nitrogen signals (compared to the bare PIRAC nitrated sample, Figure 6a) are also consistent with an organic layer having been formed by the HDPA treatment.

The external reflection FTIR spectrum of HDPA on nitrated NiTi is shown in Figure 7a. The methylene stretching modes that would be expected for a substantial HDPA coating can hardly be detected. This suggests a poorly ordered surface film. To exclude the possible effect of surface roughness on the FTIR measurements, external reflection spectra were also collected from the smooth HDPA treated TiN-sputtered on a Si wafer. The FTIR spectra of the model samples (not shown) were not different from those of the real-world alloy in Figure 7a (i.e., they too represent a disordered, poorly defined surface film).

**Anodic Oxidation of PIRAC Nitrated NiTi.** In an attempt to enhance the SAM-attachment capability of the

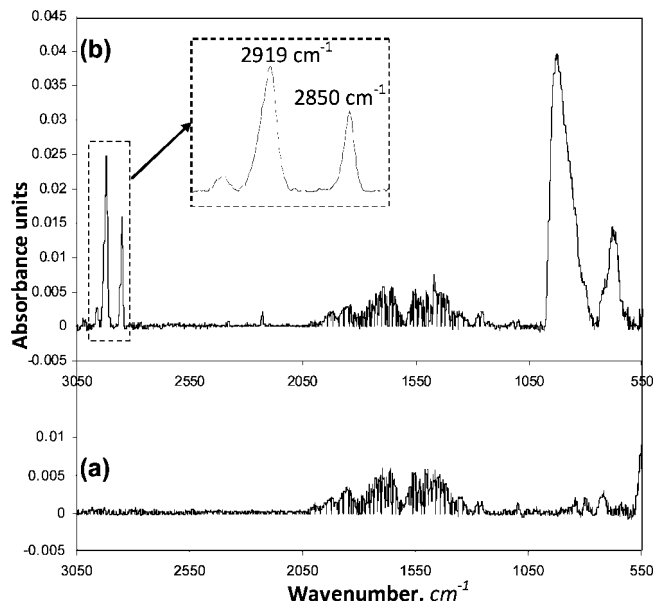


**Figure 7.** External reflection FTIR spectra of HDPA on PIRAC nitrated NiTi: (a) without anodization and (b) with anodization.

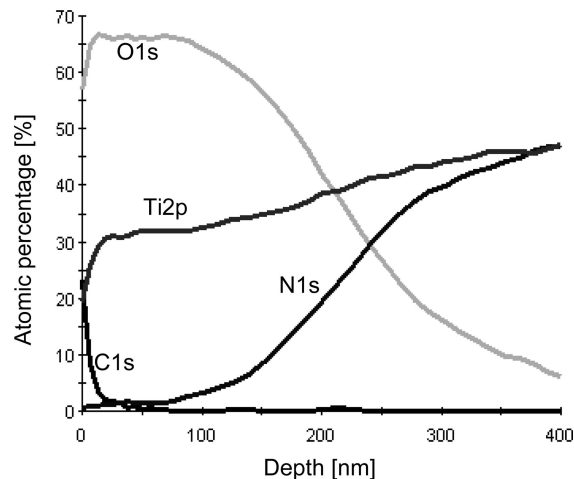


**Figure 8.** XPS depth profile of anodically oxidized PIRAC-nitrated NiTi.

nitrated surface, PIRAC nitrated NiTi samples were anodized. An XPS depth profile of anodized nitrated NiTi is shown in Figure 8. It can be seen that a rather thick ( $\sim 200$  nm) layer of Ti oxide (with traces of nitrogen) is formed on top of the titanium nitride surface. The high resolution XPS line of Ti  $2p_{3/2}$  from the anodized PIRAC nitrated NiTi (not shown) is noticeably different from that of the nonanodized material and can be neatly fit using only one peak, that of  $\text{TiO}_2$ ; that is, the anodic oxidation of PIRAC nitrated NiTi creates a single-phase  $\text{TiO}_2$  layer (of at least 100 nm) on top of the TiN surface. Additional evidence for the presence of  $\text{TiO}_2$  on the surface of anodized nitrated NiTi can be found in its FTIR spectrum (Figure 7b) which features two strong bands in the  $610\text{--}990\text{ cm}^{-1}$  region corresponding to Ti–O bonds.<sup>24</sup> The representative SEM micrograph and 3D AFM image in Figure 9 show that the anodizing of TiN-coated NiTi samples resulted in significant surface roughening ( $R_a$

(22) Hofer, R.; Textor, M.; Spencer, N. D. *Langmuir* **2001**, *17*, 4014–4020.

(23) Sieval, A. B.; Vleeming, V.; Zuilhof, H.; Sudhölter, E. J. R. *Langmuir* **1999**, *15*, 8288–8291.

(24) Velten, D.; Biehl, V.; Aubertin, F.; Valeske, B.; Possart, W.; Brems, J. J. *Biomed. Mater. Res.* **2002**, *59*, 18–28.

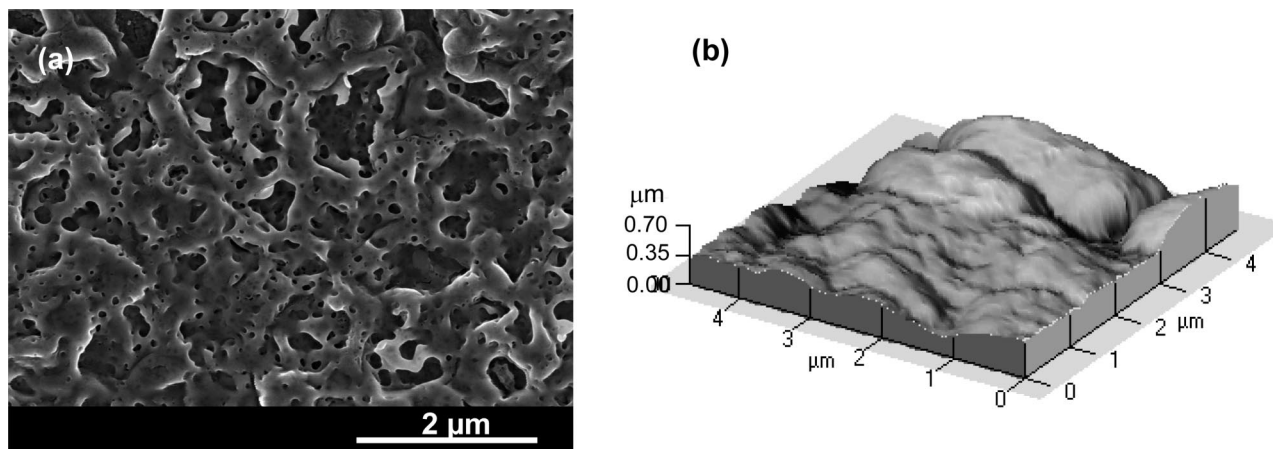


Figure 9. Surface morphology of anodized PIRAC-nitrided NiTi: (a) SEM micrograph; (b) AFM 3D image.

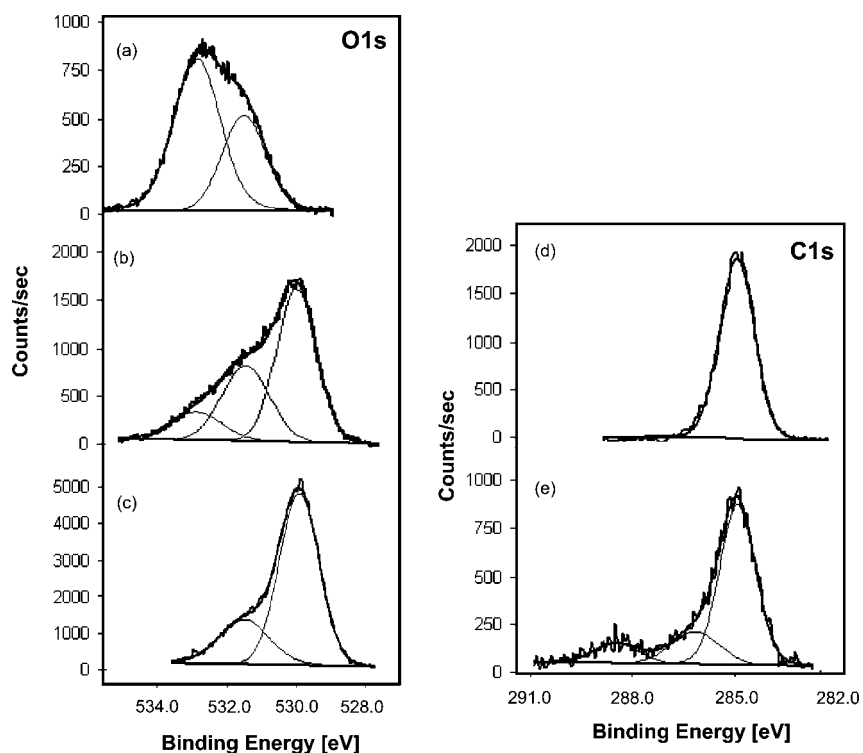


Figure 10. High resolution XPS lines (a–c) O 1s of (a) HDPa powder, (b) HDPa-treated anodized TiN-coated nitinol, and (c) anodized TiN-coated nitinol; (d, e) C 1s of (d) HDPa-treated anodized TiN-coated nitinol and (e) anodized TiN-coated nitinol.

Table 3. O 1s and C 1s Binding Energies, Full Widths at Half Maximum (FWHM) and Ratios of Deconvoluted Components for HDPa Powder and for HDPa-Treated and Bare Anodized TiN-Coated NiTi

	binding energy [eV]	FWHM [eV]	assignment	fractional peak ratio		
				HDPa powder	HDPa SAM on anodized TiN	bare anodized TiN
O 1s	530.1 ± 0.1	1.4	TiO <sub>2</sub>		0.55	0.75
	531.6 ± 0.1	1.6	P=O P=O; P–O–Ti	0.34	0.32	
	533.0 ± 0.1	1.7	surface contaminations: OH; C=O; C–O–C P–OH P–O–H	0.66		0.25
C 1s	285.0 ± 0.1	1.4	C–H	1 (not shown)	1	0.70
	286.5 ± 0.1	1.6	contaminations: C–OH; C=O; C–O–C			0.19
	288.6 ± 0.1	1.6				0.11

= 115 and 44 nm after and before anodizing, respectively). This relatively large roughness did not preclude the precise analysis of an organic monolayer deposited on this anodized surface (below).

#### HDPa Attachment to Anodized, PIRAC Nitrided NiTi.

The external reflection FTIR spectrum of an HDPa-treated anodized-TiN surface is shown in Figure 7b. Strong methylene modes at 2919 cm<sup>-1</sup> and 2850 cm<sup>-1</sup> for the asym-

metric and symmetric stretches, respectively, indicate a densely packed well-ordered HDPA monolayer similar to the one formed on anodized Ti45Nb.<sup>10</sup>

The XPS survey spectrum of anodized, nitrided, NiTi treated with HDPA (further referred to as HDPA-TiO<sub>2</sub>) is shown in Figure 6c. The P 2p peak (associated with HDPA) is stronger than that which is obtained with the nonanodized samples, Figure 6b (further referred to as HDPA-TiN). The Ti 2p peak (originating from the substrate) is weaker in the sample where the TiN was anodized, Figure 6c, suggesting a more complete HDPA coverage on HDPA-TiO<sub>2</sub>. On the other hand, the larger inelastic background at the higher binding energy side of the Ti 2p line observed in the spectrum of HDPA-TiN (Figure 6b) would mean a thicker layer of HDPA on the nonanodized sample.<sup>25–27</sup> We hypothesize that this discrepancy points to the fact that the organic coating on the TiN surface is a thick nonuniform layer of loosely bound HDPA molecules and other organic contaminants, while the HDPA monolayer formed on the TiO<sub>2</sub>-coated TiN surface is a densely packed, albeit thin, monolayer.

Similar to our previous work,<sup>10</sup> the existence of phosphonate–substrate covalent bonding was established by comparing the high resolution XPS O 1s lines of HDPA powder (Figure 10a) with those of HDPA-treated and bare anodized TiN-coated NiTi (Figure 10b,c), respectively. The O 1s line of the anodized sample could be fitted using two peaks, one corresponding to TiO<sub>2</sub> (530.1 eV) and the other to carbon-containing surface contamination and adsorbed hydroxyl groups (531.6 eV; Table 3). As suggested by the analysis of the corresponding C 1s lines (Figure 10d,e), the carbon-containing contaminants are removed from the surface during HDPA deposition and are exchanged by adsorbed HDPA molecules. It can therefore be assumed that the two peaks detected (in addition to TiO<sub>2</sub>) in the O 1s line of the HDPA-treated substrate (Figure 10b) are associated with the phosphonic acid group (PO(OH)<sub>2</sub>). Indeed, these two peaks appear at the same binding energies (531.6 and 533.0 eV) as the O=P and P–O–H peaks of the HDPA powder (Figure 10a). The ratio of these two peaks, however, is significantly different: 0.52 versus 2.5 for unbound HDPA molecules and HDPA-treated anodized NiTi, respectively. The former value is what is expected for the stoichiometric 2-to-1 ratio of the O=P and P–OH oxygens in a free phosphonic acid. The larger proportion of the peak at 531.6 eV (assigned also to P–O–Ti bonds) in the O 1s line from HDPA-treated anodized NiTi must be due to the disappearance of most of the P–OH bonds (533.0 eV) and the formation of P–O–Ti covalent bonds between HDPA molecules and titanium oxide surface. Similar changes within the XPS line of O 1s have been recently reported for covalent binding of phosphonic acid monolayers to Ti and Ti-Nb alloy surfaces.<sup>10,28</sup>

These results clearly show that a significant difference exists in the HDPA attachment capability of anodically oxidized and nonoxidized TiN-coated surfaces. While (based

on the FTIR data in Figure 7 and on the analogy to previous work from our laboratory<sup>12</sup>) a well-ordered organic monolayer was formed on the oxide surface, little if any HDPA attachment occurred on the nitride surface. The low surface coverage of alkylphosphonic acid on a Ti nitride surface can be explained by adopting the mechanism proposed by Textor et al.<sup>29</sup> and Schwartz et al.<sup>8</sup> for the successful attachment of phosphonic acid monolayers on Ta oxide and Ti oxide, respectively. In this mechanism, covalent bonding and self-assembly of phosphonate molecules on the TiO<sub>2</sub> surface becomes possible due to the surface OH group regeneration via proton transfer from the phosphonic group to the surface oxygen. In the case of our TiN surface, OH group regeneration only occurs when there is an oxygen atom close to the phosphonic hydrogen, whereas no such regeneration is possible if the next neighbor is nitrogen. The high surface concentration of nitrogen (Table 1) severely curtails the possibility of OH regeneration on TiN-coated NiTi (Table 1), and phosphonate attachment mostly occurs by consumption of the existing surface OH groups. It is reasonable that the surface OH content of a TiN coating is even lower than that of the native Ti oxide, and this explains the low HDPA coverage observed on our nitrided surfaces.

## Conclusions

The main thrust of the present work was to obtain a SAM of an alkylphosphonic acid (HDPA) on PIRAC nitrided NiTi alloy (Nitinol) as a first step toward biofunctionalization of this surgical metal. The PIRAC-grown nickel-free Ti nitride coating is expected to enhance the biocompatibility of Nitinol by improving its corrosion resistance and limiting the release of harmful Ni ions. Despite the oxygen content of the topmost surface, little if any HDPA attachment occurred on PIRAC-nitrided NiTi alloy. The formation of a densely packed uniform HDPA monolayer was made possible by anodizing the nitrided surface prior to HDPA deposition. Unlike the anodizing of bare NiTi alloy that cannot produce dense Ti oxide layers due to Ni dissolution, the anodizing of PIRAC nitrided NiTi yielded a ~100 nm thick TiO<sub>2</sub> coating on top of the TiN. FTIR and XPS measurements verified the ability to establish a covalently attached phosphonate SAM on such a surface. The use of related SAMs (with functional groups at the other end of the alkyl chain) for surface modification of the NiTi with biologically active molecules is currently under investigation.

**Acknowledgment.** We acknowledge the financial support of GIF Research Grant I-810-236.10/200, of the Commission of the European Communities, Network of Excellence (EXCELL) No. 515703, of the Bar Ilan Minerva Center for Biomaterial Interfaces and of the Edward and Judy Steinberg Chair in Nanotechnology at Bar Ilan University.

CM703710Q

(25) Hansen, H. S.; Tougaard, S.; Biebuyck, H. J. *Electron Spectrosc. Relat. Phenom.* **1992**, *58*, 141–158.

(26) Tougaard, S. *Appl. Surf. Sci.* **1996**, *100/101*, 1–10.

(27) Castle, J. E.; Chapman-Kpodo, H.; Proctor, A.; Salvi, A. M. *J. Electron Spectrosc. Relat. Phenom.* **2000**, *106*, 65–80.

(28) Adden, N.; Gamble, L. J.; Castner, D. G.; Hoffman, A.; Gross, G.; Menzel, H. *Langmuir* **2006**, *22*, 8197–8204.

(29) Textor, M.; Ruiz, L.; Hofer, R.; Rossi, A.; Feldman, K.; Hähner, G.; Spencer, N. D. *Langmuir* **2000**, *16*, 3257–3271.